# Structure of $^{18}$Ne

A. V. Nero* and E. G. Adelberger†
*Stanford University, Stanford, California 94305 and Princeton University, Princeton, New Jersey 08540*

F. S. Dietrich
*University of California, Lawrence Livermore Laboratory, Livermore, California 94550*

(Received 30 July 1980; revised manuscript received 1 June 1981)

We have studied $^{18}$Ne states up to 9 MeV excitation energy via the $^{16}$O($^3$He,$n$)$^{18}$Ne and $^{20}$Ne($p,t$)$^{18}$Ne reactions. Excitation energies, widths, absolute cross sections, and angular distributions were measured. Distorted-wave Born approximation calculations were performed for comparison with the ($^3$He,$n$) angular distributions and the ($p,t$) data were compared with previous calculations. Members of the 4.5-MeV doublet were found to have excitation energies of $4.518 \pm 0.008$ and $4.590 \pm 0.008$ MeV with spin and parity $1^-$ and $0^+$, respectively. The 5.1-MeV group was resolved into a doublet with $5.090 \pm 0.008$ and $5.144 \pm 0.008$ MeV excitation energies. Several previously unidentified states were found at excitation energies greater than 5 MeV, including a state at $7.062 \pm 0.012$ MeV that is strongly populated via ($^3$He,$n$), but not observed in ($p,t$). We calculated two-particle Coulomb energy shifts for model mass-18 $T = 1$ states and found that the difference between the excitation energy of the 4.59-MeV $0^+$ state and the analogous state at 5.34 MeV in $^{18}$O gives strong evidence for the predominantly $s_{1/2}{}^2$ character of the state.

[NUCLEAR REACTIONS, NUCLEAR STRUCTURE
$^{16}$O($^3$He,$n$)$^{18}$Ne, $E = 10-22$ MeV; measured $\sigma(E_n,\theta)$. $^{20}$Ne($p,t$)$^{18}$Ne, $E = 41.8$ MeV; measured $\sigma(E_t,\theta)$. Gas targets. DWBA analysis. Deduced $^{18}$Ne levels, J, $\pi$. Calculated Coulomb shifts for model mass 18 $T = 1$ states.]

## I. INTRODUCTION

Many calculations have attempted to reproduce low-lying level energies and other observables of the mass 18 nuclei by constructing configurations with two particles in the $2s\,1d$ shell outside a closed $^{16}$O core. For the case of $T = 1$ states, several investigators[1–4] successfully reproduced the five lowest experimental level positions of $^{18}$O (see Fig. 1). However, the existence of third $0^+$ and $2^+$ states at 5.2 MeV excitation energy demonstrates the inadequacy of this picture, since in a spherical shell model the third $0^+$ state (designated $0_3^+$) should occur around 10 MeV excitation, twice the $d_{5/2} - d_{3/2}$ splitting in mass 17. Furthermore, the large $E2$ transition rates in $^{18}$O, particularly the $0_2^+ \rightarrow 2_1^+$ rate, raise serious doubts as to the character of even the states below 4 MeV[2].

These difficulties suggest the presence of substantial deformed components in states at low excitation energy. These might be constructed, for example, by removing two $p$-shell particles from members of the $^{20}$Ne ground state rotational band. Such configurations are explicity included in the bases of several calculations.[6–11] The states obtained using these larger spaces have energies that correspond well with low-lying levels and yield reasonable gamma transition rates[7,10,12]; the general amount of mixing between two-particle and deformed configurations does not vary greatly among the authors. However, important differences can be found, resulting from different choices for unmixed configuration energies and for off-diagonal matrix elements. The most striking difference is that some calculations[6,10] result in a $0_2^+$ wave function whose intensity is 70% deformed component, while others[7,13] present $0_3^+$ as deformed, with $0_2^+$ essentially two particle. In spite of these differences, both sets of calculations yield gamma transition rates that agree reasonably well with the ex-

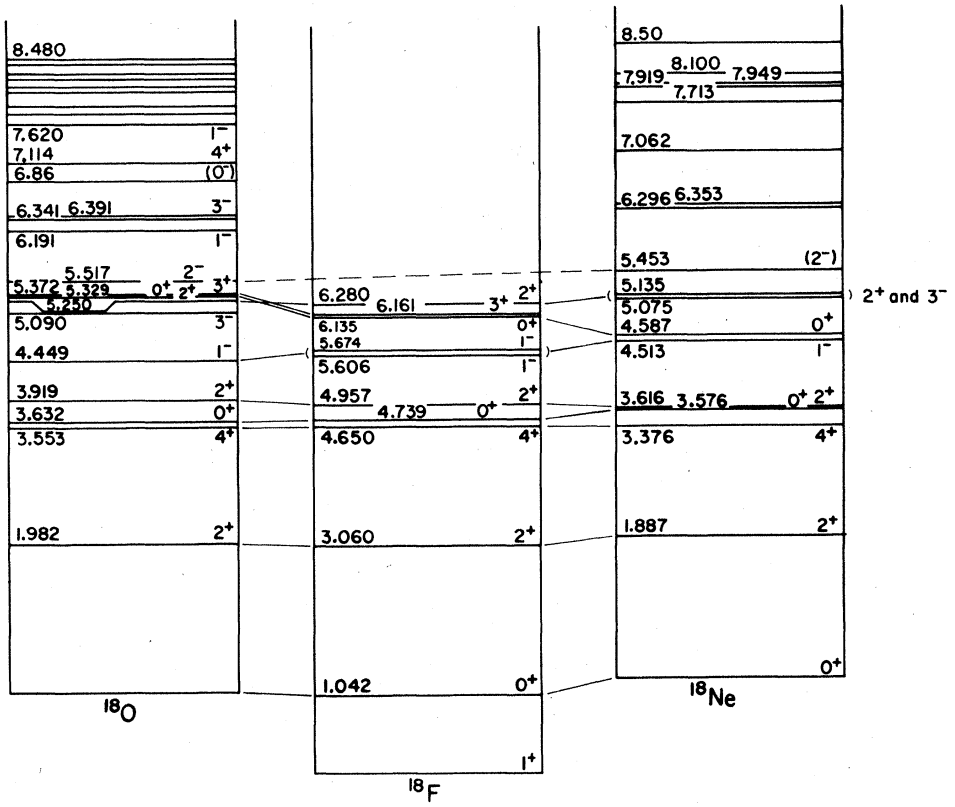


FIG. 1. $T = 1$ states in mass 18 (from Ref. 5 as well as recent work, including that of this paper).

perimental values.

Two-particle transfer strengths depend strongly on wave functions, and it might be thought that these would provide a decisive test in the case of mass 18. Currently, though, experimental results are incomplete, and comparison with two-particle calculations in the distorted wave Born approximation (DWBA) yields ambiguous results. On the basis of such a comparison, the limited $^{16}O(t,p)^{18}O$ data available[14] have been found[15] to favor the wave functions of Benson and collaborators,[10,16] which characterize $0_2^+$ as primarily deformed; unfortunately, the wave functions of Engeland,[7] which are quite different, were not tested in Ref. 15. An analysis[17] of $^{20}Ne(p,t)^{18}Ne$ data found the results of both Refs. 7 and 10 satisfactory, with those of Engeland slightly favored. Additional measurements of transfer strengths to $T = 1$ states in mass 18 and more complete analysis of the results would be helpful.

Although the Coulomb energies of $T = 1$ multiplets have been a subject of interest for some time,[18–20] they have not been exploited as a tool to obtain structural information. We show below that relative energy shifts in mass 18 can be related to the configurations present in the wave functions of the states considered, and that the Coulomb energies can be used to rule out decisively certain proposed wave functions of the mass 18 nuclei.

Interpretation of two-particle stripping strengths or energy shifts in the $T = 1$ states of mass 18 requires a well-determined level scheme of the $T = 1$ multiplets. Prior to our work this was not available for $^{18}$Ne. The $^{16}O(^3He,n)^{18}Ne$ reaction had been used at low energies to determine spin and parity ($J^\pi$) of the ground and first few states.[21–23] More recently, Towle and Wall[24] studied states up to 4.59 MeV excitation energy, and Adelberger and McDonald[25] up to 5.14 MeV. The comparison of observed angular distributions with DWBA calculations, and results from the $^{16}O(^3He,n\gamma)$ $^{18}$Ne reaction,[26–28] fixed $J^\pi$ for the five particle-stable states, i.e., below 3.9 MeV. The character of the doublet[25] at 4.5 MeV and the state at 5.1 MeV were undetermined, although Ref. 25 suggested that one member of the 4.5 MeV doublet was the analog of the 5.2 MeV $0_3^+$ state of $^{18}$O. The $^{20}Ne(p,t)^{18}Ne$ reaction, which should populate a somewhat different group of states than ($^3$He,$n$), was studied by a number of workers,[17,29–31] who reported states at approximate-

ly 4.5, 5.1, 6.3, 8.0, and 9.2 MeV. Although these studies failed to resolve either the 4.5 or 5.1 MeV doublet, they suggested $J^\pi = 1^-$ for the 4.5 MeV "state", and $J^\pi = 3^-$ or a combination of $3^-$ and $2^+$ for the 5.1 MeV "state".

We have investigated the $^{16}$O($^3$He, $n$)$^{18}$Ne reactions at beam energies from 10 to 22 MeV to study states in $^{18}$Ne up to 9 MeV excitation. Excitation energies, widths, absolute cross sections, and angular distributions have been obtained. Angular distributions from the strongly populated states are compared with DWBA calculations. Special care has been taken in the study of the states at 4.5 and 5.1 MeV because, as discussed later, determination of their spin and parity and comparison of their excitation energies with those of analogous states in $^{18}$O can put a strong constraint on possible sets of wave functions for mass 18. Some attention has also been given to the possibility of observing states (possibly as low as 7 MeV) to which the $d_{3/2}$ orbital contributes in a major way.

We have also studied the $^{20}$Ne($p,t$)$^{18}$Ne reaction at a beam energy of 41.8 MeV. In these measurements, which were particularly intended to characterize the states at 4.5 and 5.1 MeV, a somewhat different set of states was populated than in the ($^3$He,$n$) work.

Preliminary results of this work have already been presented in brief form[32–34] and demonstrate that most of the two-particle $s_{1/2}{}^2$ strength lies in the third $0^+$, $T = 1$ state rather than the second. This conclusion has since been confirmed by a reexamination of particle transfer strengths[35] and of these data together with gamma transition strengths.[36] In new calculations of mass 18 spectra and transition rates, it is therefore appropriate to require that $0_3^+$ contains much of the $s_{1/2}{}^2$ strength, as was done in Ref. 37. Our experimental measurements are also beginning to be confirmed at other laboratories.[38]

## II. THE $^{16}$O($^3$He,$n$)$^{18}$Ne REACTION

### A. Experimental procedure

#### *1. The time-of-flight system*

Our study of the $^{16}$O($^3$He,$n$)$^{18}$Ne reaction employed the time-of-flight spectrometer[39] associated with the Stanford FN tandem Van de Graaff accelerator. The beam is pulsed by a 3.5 MHz chopper that sweeps the high energy beam over the vertical object slits before the 90° analyzing magnet. The current passing between the slits is increased by bunching the low energy dc beam and automatically regulating the phase between the buncher and chopper. Over a wide range of energies, the system produces 100 to 200 nA of a time-averaged $^3$He beam on target, with a 2 nsec long pulse arriving every 286 nsec.

Neutrons are detected in a 5.1 cm thick $\times$ 12.7 cm diam plastic scintillator coupled to an Amperex XP1040 phototube. The detector is placed in a large lead and $LiCO_3$-loaded-paraffin collimator that shields the detector from room background gamma rays and neutrons. A 1.27 cm thick lead plate in front of the detector attenuates low energy gamma rays from the target.

Two signals are derived from the phototube: a large fast anode pulse, which starts the time-to-amplitude converter (TAC), and a slow linear dynode pulse. Events are stored only if the linear pulse exceeds some minimum level, so that the effect of phototube noise may be minimized and a bias may be set against low energy neutrons and gamma rays. The stop pulse for the TAC is derived from an rf pickup loop at the chopper. The phase of this signal is normally adjusted so that the peak due to prompt gamma radiation from the target is in the high-channel portion of the spectrum. Flight time therefore increases in the low-channel direction. The time resolution of the dectector is $\simeq 1$ nsec, exclusive of the effect of scintillator thickness, for the bias setting used in this work.

TAC output pulses are analyzed by a computer-controlled analog-to-digital converter (ADC). The computer eliminates the effect of long-term time drifts in the beam-pulsing and detector systems by a digital feedback scheme that adjusts the zero of the TAC spectrum to stabilize the centroid of the prominent peak due to prompt gamma rays. A Fortran program also provides other features convenient for interpretation of any of the time spectra in the memory. Most important is the ability to calibrate the time scale internally and identify unknown groups. Moreover, the area under peaks can be obtained, and spectra can be manipulated or plotted with an excitation energy scale such as that seen in the figures in this work. These features, which may be used while a spectrum is being accumulated, do not contribute to the ADC dead time.

#### *2. Target*

The design of the gaseous $^{16}$O target is shown in Fig. 2. Gas contained in the gold-lined stainless

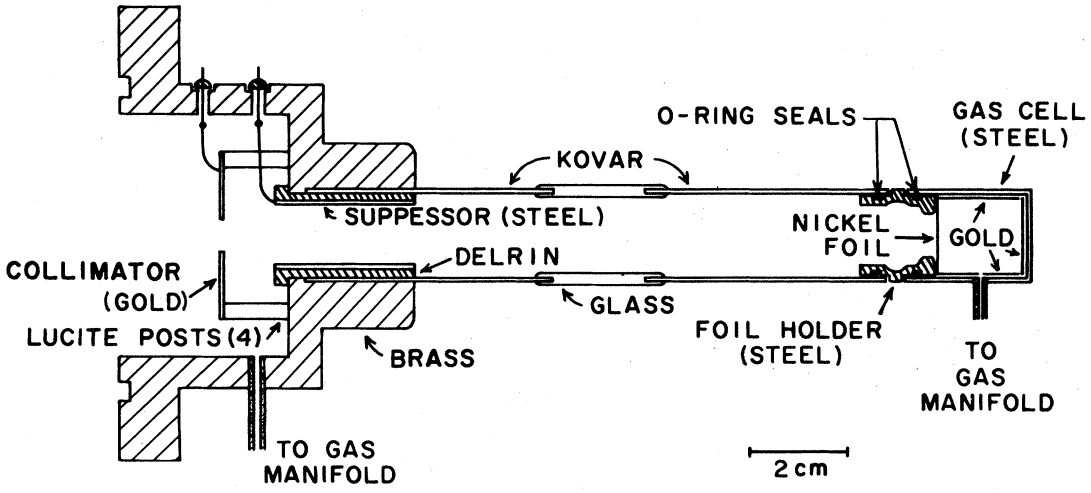


FIG. 2. Gas target arrangement. Beam enters from the left.

steel cell at the right is isolated from the beam tube by a nickel foil $\simeq 9 \times 10^{-5}$ cm thick. The cell also serves as a Faraday cup for beam integration. Materials are chosen so that the cell and holder yield minimum background in the accumlated spectra. For the present work, the cell was filled with natural oxygen (purity $\geq$ 99.6%) to a pressure of 25 to 150 Torr. All bombarding energies given in this work refer to the beam energy at the center of the gas cell after correcting for energy loss in the entrance foil and target gas. Losses in the foil were found by scaling the measured energy losses of 5.45 MeV alpha particles from $^{241}$Am.

### 3. *Neutron detection efficiency*

The absolute neutron detection efficiency was obtained using known cross sections[40] for the $^2$H$(d,n)^3$He reaction. The gas target cell for the $^2$H$(d,n)$ measurements was very similar to that employed for the $^{16}$O$(^3$He,$n)$ work. Relative detection efficiencies for low energy neutrons were obtained from the $^3$H$(p,n)^3$He reaction using a target of tritium absorbed onto zirconium. Cross sections were taken from Refs. 41 and 42. As seen in Fig. 3, the results from the two sets of tritium data are in only moderate agreement; the difference does not appear to be due to the experimental procedure of the present work. We have normalized the mean of the results from the tritium data to those from the $^2$H$(d,n)$ data, as shown in the figure. The solid curve shows the function used in analysis of the $^{16}$O$(^3$He,$n)$ data. The sample 5% error bars, which indicate the desired precision for *relative* efficiencies, are smaller than the fluctuations of individual data points from the curve. In addition, an overall absolute uncertainty of 10% must be added to the error shown. Owing to ambiguities in tails on neutron peaks arising from scattering in the detector shield, possible errors in the target thickness measurements, and inaccuracies in charge integration, the total uncertainty in absolute cross sections is taken to be 15%.

## B. Experimental results

### 1. *States observed*

The excitation energy and width of states populated in a neutron-producing reaction are most easily measured by comparing the group of interest with a group produced in a known reaction and adjusting beam energies so that the known and unknown groups have approximately the same neutron energy. In the present work, the low-lying levels of $^{18}$Ne as measured in the $^{16}$O$(^3$He,$n\gamma)$ work of Robertson *et al.*[26] were used as standards. Since the unknown and standard reactions are the same, uncertainty in the $Q$ value for the $^{16}$O$(^3$He,$n)^{18}$Ne reaction does not affect excitation energy measurements.

Time spectra in Figs. 4—7, accumulated at bombarding energies from 10 to 18 MeV, exhibit states below 9 MeV excitation energy in $^{18}$Ne. The excitation energy scales shown in these figures are only approximate and assume linearity of the time scale. In each case, the time scale was calibrated using the position of the prompt gamma ray (channel 244) and of some particular state in $^{18}$Ne, yielding approximately 1.1 nsec/channel. Groups due to the

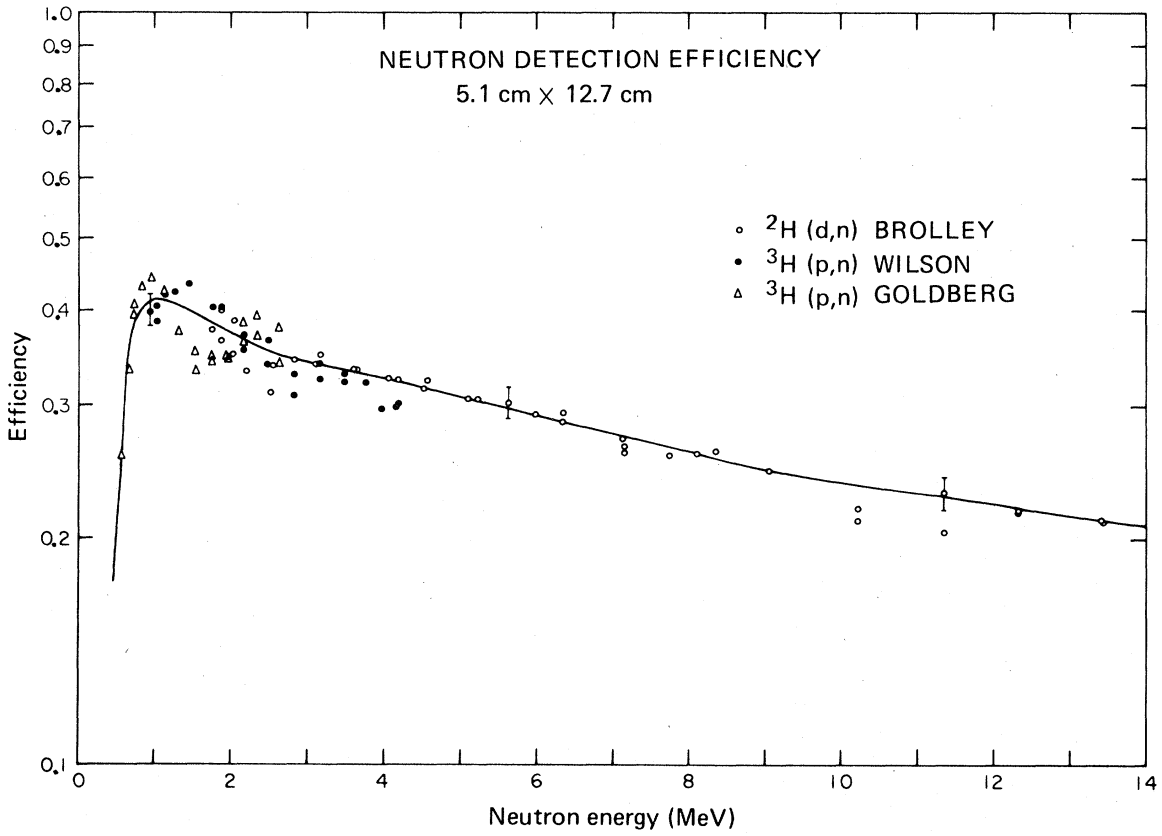


FIG. 3. Neutron detection efficiency. The data points are based on previously measured absolute $^2$He($d,n$) and $^3$H($p,n$) cross sections. The solid line indicates the efficiency function used in the data analysis of this work.

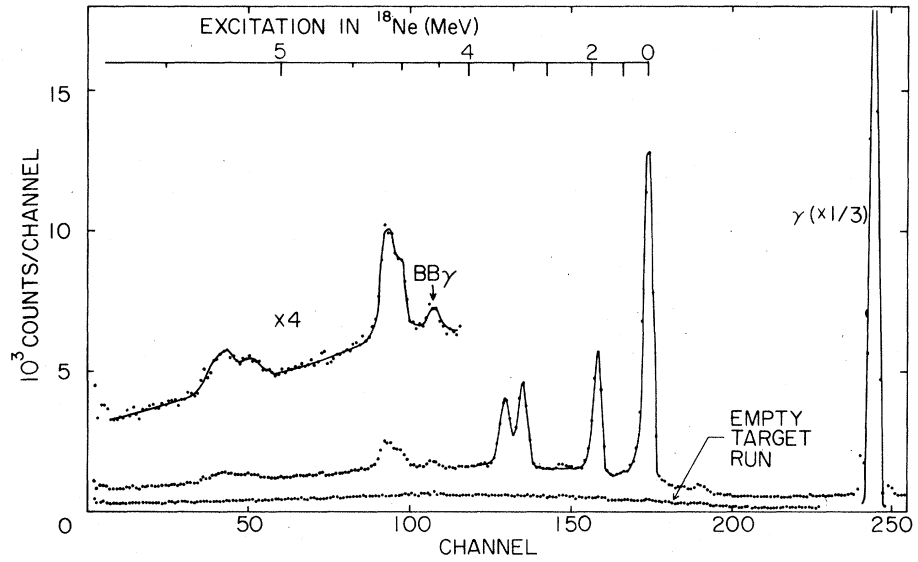


FIG. 4. Time spectrum for $^{16}$O($^3$He,$n$)$^{18}$Ne at 10.52 MeV, 3.0 m, 5°. The peak labeled BB$\gamma$ is the prompt $\gamma$ ray due to an out-of-phase beam burst. The background run shown was accumulated for approximately $\frac{1}{3}$ as much integrated beam as the foreground run. Lines are drawn to guide the eye.

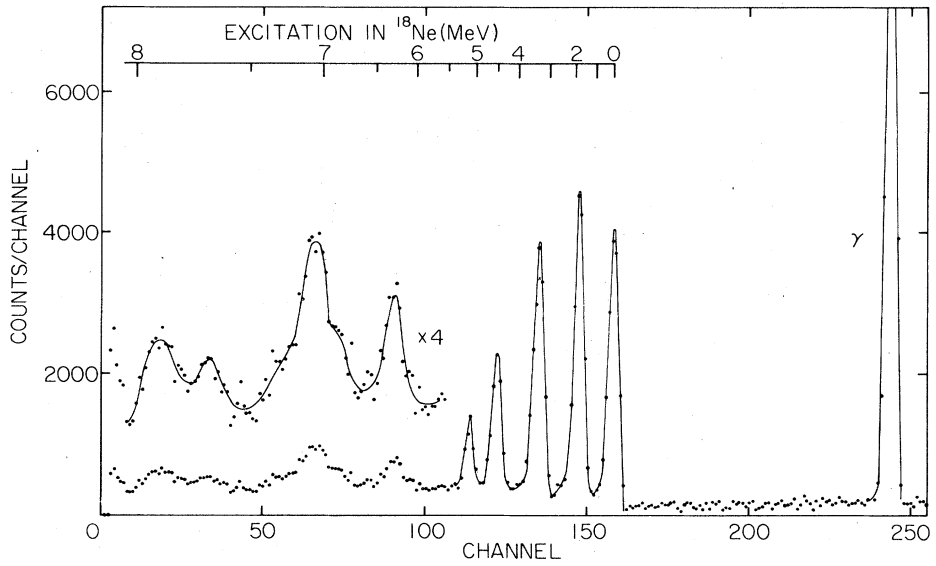


FIG. 5. Time spectrum for $^{16}$O($^3$He,$n$)$^{18}$Ne at 14.51 MeV, 4.74 m, 5°. A background run has been subtracted.

ground state (g.s.) and 1.89 MeV state are resolved in all cases. At the lower beam energies, the 3.36 MeV group is partially resolved from a group due to the doublet at 3.6 MeV, but at higher energies these three states appear as one group. For $^3$He energies below 11 MeV, the groups at 4.5 and 5.1 MeV are seen to be due to doublets. At higher energies, additional states appear at excitation energies near 6.3, 7.1, 8.0 (a triplet), and 8.5 MeV. Although some spectra suggest that the states near 6.3 and 7.1 MeV have structure (e.g., Fig. 5), attempts to verify this were inconclusive, and in analysis of the ($^3$He,$n$) data they are treated as structureless, broad states. Spectra at bombarding energies greater than 18 MeV contained substantial yields of neutrons corresponding to excitation energies in $^{18}$Ne greater than

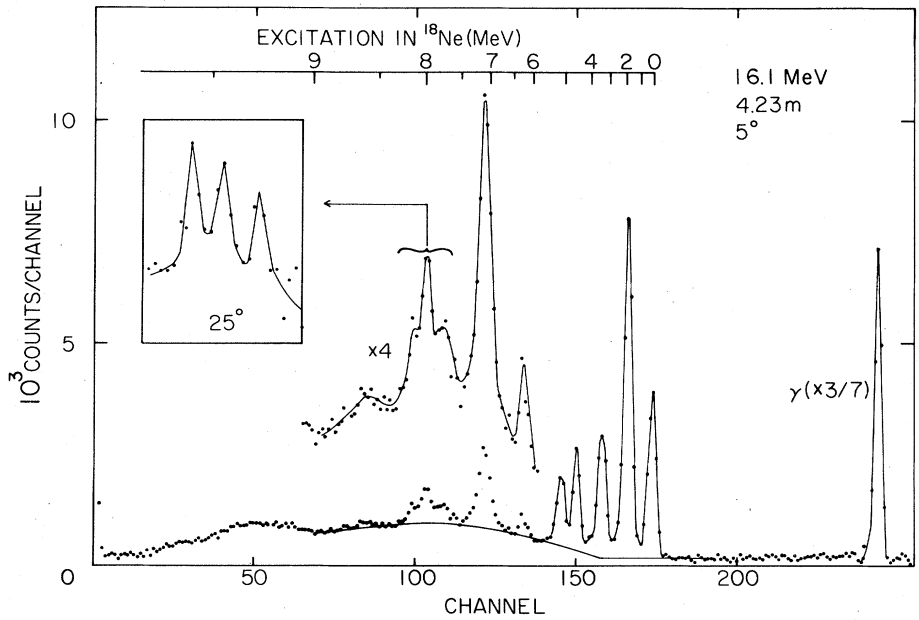


FIG. 6. Time spectrum for $^{16}$O($^3$He,$n$)$^{18}$Ne at 16.1 MeV, 4.23 m, 5°. A background run has been subtracted. The insert shows the 8 MeV triplet at another angle. Peak areas were taken above the smooth curve shown, which simulates the yield from random background and from three-body final states.

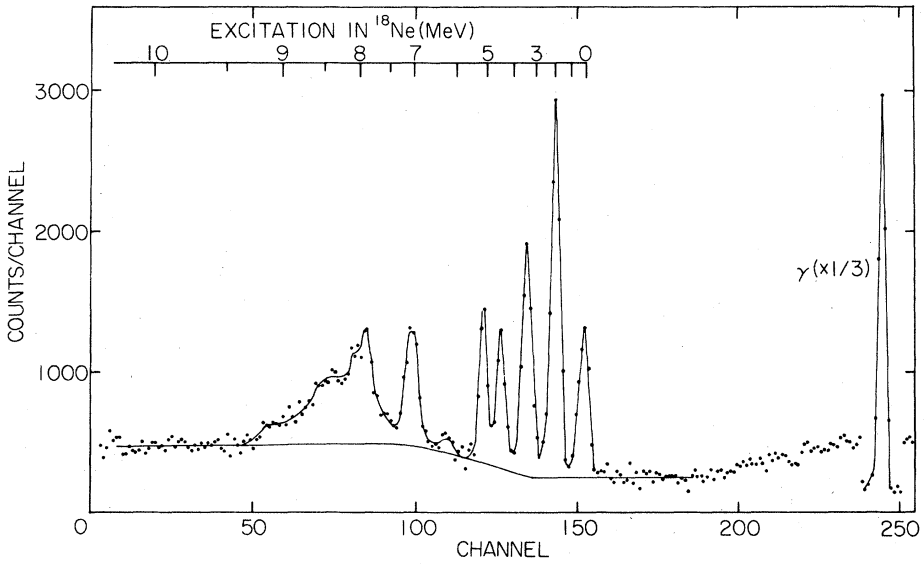


FIG. 7. Time spectrum for $^{16}$O($^3$He,$n$)$^{18}$Ne at 17.8 MeV, 6.14 m, 5°. A background run has been subtracted. Areas were obtained above the smooth curve.

9 MeV. A system with better resolution than that at Stanford is required for study of this region.

Cross sections for some of the strongly populated states have been plotted in Fig. 8. As expected, cross sections at beam energies from 14 to 22 MeV show no evidence for resonances in the compound system.

Our measured widths and excitation energies are summarized in the first column of Table I. Quoted errors in the excitation energies are computed from uncertainties in the peak positions and in the relative beam energies for the unknown and calibration spectra. Estimates for the width of the "unknown" states were obtained by comparing their observed widths with those of "known" states with similar neutron energies.

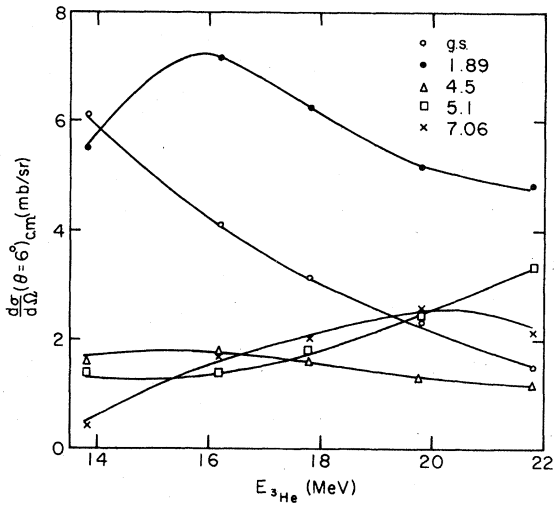


FIG. 8. Approximate 6° cross sections of strong states for beam energies from 14 to 22 MeV.

None of the "$^{18}$Ne levels" listed in Table I arises from ($^3$He,$n$) reactions on impurities in the $^{16}$O target. Subtraction of empty target spectra accumulated under conditions identical to the full target run eliminates groups from sources other than the target gas, such as collimators, entrance foil, or beam stop. Impurities in the target gas would produce groups with shorter flight times than $^{18}$Ne (0.0), since ($^3$He,$n$) reactions on all other targets have more positive $Q$ values than on $^{16}$O. No such groups were seen after empty target subtractions were performed.

A study of neutron energy versus angle for each of the groups in the figures gave results consistent with an $^{16}$O target. For each angle in a series of spectra taken at 16.1 MeV, excitation energies were calculated assuming a variety of targets. Examination of the kinematic shifts indicated that the 7.06, 7.71, and 8.10 MeV states are due to a mass 16 target, the 6.29 MeV state to mass 15 or 16, and the 7.92 MeV level to mass 15 to 17. From all the evidence, we conclude that the observed groups arise from the $^{16}$ O($^3$He,$n$)$^{18}$Ne reaction.

### *2. Angular distributions*

Angular distributions of neutrons populating many of the states in $^{18}$Ne are shown in Figs. 9 to 11.

TABLE I. Excitation energies in $^{18}$Ne.[a]

| | Present work | | Previous results[b] | |
|---|---|---|---|---|
| | $^{16}$O($^3$He,$n$)$^{18}$Ne | $^{20}$Ne($p,t$)$^{18}$Ne | $^{16}$O($^3$He,$n$)$^{18}$Ne | $^{20}$Ne($p,t$)$^{18}$Ne[c] |
| 1 | | 1.886(10) | 1.8873(0.2)[d] | 1.890(20) |
| 2 | | 3.375(10) | 3.3762(0.4)[d] | 3.375(30) |
| 3 | | 3.580(10) | 3.576(2)[d] | 3.588(25) |
| 4 | | 3.612(10) | 3.6164(0.6)[d] | |
| 5 | 4.513(13) | 4.522(10), $\leq$ 20 | 4.505(15), $\leq$ 40[e] | 4.55 (20) |
| 6 | 4.587(13) | 4.592(10), $\leq$ 20 | 4.571(15), $\leq$ 40[e] | |
| 7 | 5.075(13), $\leq$ 60 | 5.099(10), 40 $\pm$ 20 | 5.14(20), 100 $\pm$ 40[e] | 5.14 (20) |
| 8 | 5.135(12), $\leq$ 60 | 5.151(10), 25 $\pm$ 15 | | |
| 9 | | 5.453(10), $\leq$ 50 | | |
| 10 | 6.291(30), 180 $\pm$ 60 | 6.297(10), $\leq$ 60 | | 6.38 (20) |
| 11 | | 6.353(10), $\leq$ 60 | | |
| 12 | 7.062(12), 180 $\pm$ 50 | | | |
| 13 | 7.712(20), $\leq$ 50 | 7.713(10), $\leq$ 60 | | |
| 14 | 7.915(12), $\leq$ 50 | | | |
| 15 | | 7.949(10), $\leq$ 60 | | 7.957(25) |
| 16 | 8.100(14), $\leq$ 50 | | | |
| 17 | 8.50 (30), $\leq$ 120 | | | |
| 18 | | 9.198(10), $\leq$ 60 | | 9.17 (30) |

[a]Each entry is presented in the form: energy (uncertainty), width. The units are MeV (keV), keV.
[b]Brackets indicate unresolved doublets.
[c]Most precise results are given in Ref. 5, with exception of 7.96 MeV state, which is taken from Ref. 31.
[d]Reference 26.
[e]Reference 25.

The smooth curves are the result of calculations discussed in Sec. IV.

Figure 9 shows results for beam energy 13.8 MeV and a flight path of 3 m, selected to study the doublets at 4.5 and 5.1 MeV. Fitting the 4.5 MeV group with a single Gaussian peak required a substantial change of width with angle, an expected result when components of a doublet change their relative strengths with angle. At angles less than 30° this group was found to be 0.5 channels narrower and have an apparent excitation energy $\simeq$ 30 keV higher than at larger angles. This suggests that at the maximum in the angular distribution of Fig. 9 the group is dominated by the higher-lying member of the doublet and that at large angles the two contributions become comparable. The 5.1 MeV group did not show such obvious variation of peak width or excitation energy with angle. However, careful measurements at 0° of the apparent excitation energy of the group, with beam energies of 14 MeV, give a result 5.133 $\pm$ 0.012 MeV, which is high enough to suggest that the 5.135 MeV state dominates the group at small angles.

Figure 10 displays an angular distribution taken at 16.1 MeV. The flight path was 4.25 m for angles $\leq$ 40° and 3.1 m for angles $>$ 40°. Superimposed on these data are the results from an independently analyzed angular distribution at 16.3 MeV with a flight path of 3 m. The latter results have not been normalized to the 16.1 MeV data, except that the yield to the ground state has been increased by 4% because of the observed cross-section variation with beam energy as seen in Fig. 8. Because the groups of interest are not as well resolved at these energies, estimating the continuum yield to three-particle final states introduces a significant uncertainty, included in the results of Fig. 10. The curve in Fig. 6 (the 5° spectrum of the 16.1 MeV angular distribution) is drawn to account for this yield and is typical of the shapes observed for ($^3$He,$n$) reactions in this mass region.

An angular distribution was taken at 17.8 MeV with a 6 m flight path to obtain data at as high outgoing neutron energy as possible. The 5° spectrum is displayed in Fig. 7. Cross sections are given in Fig. 11.

## III. THE $^{20}$Ne($p,t$)$^{18}$Ne REACTION

### A. Experimental procedure

We studied the $^{20}$Ne($p,t$)$^{18}$Ne reaction using a gas target and a solid state detector telescope in the

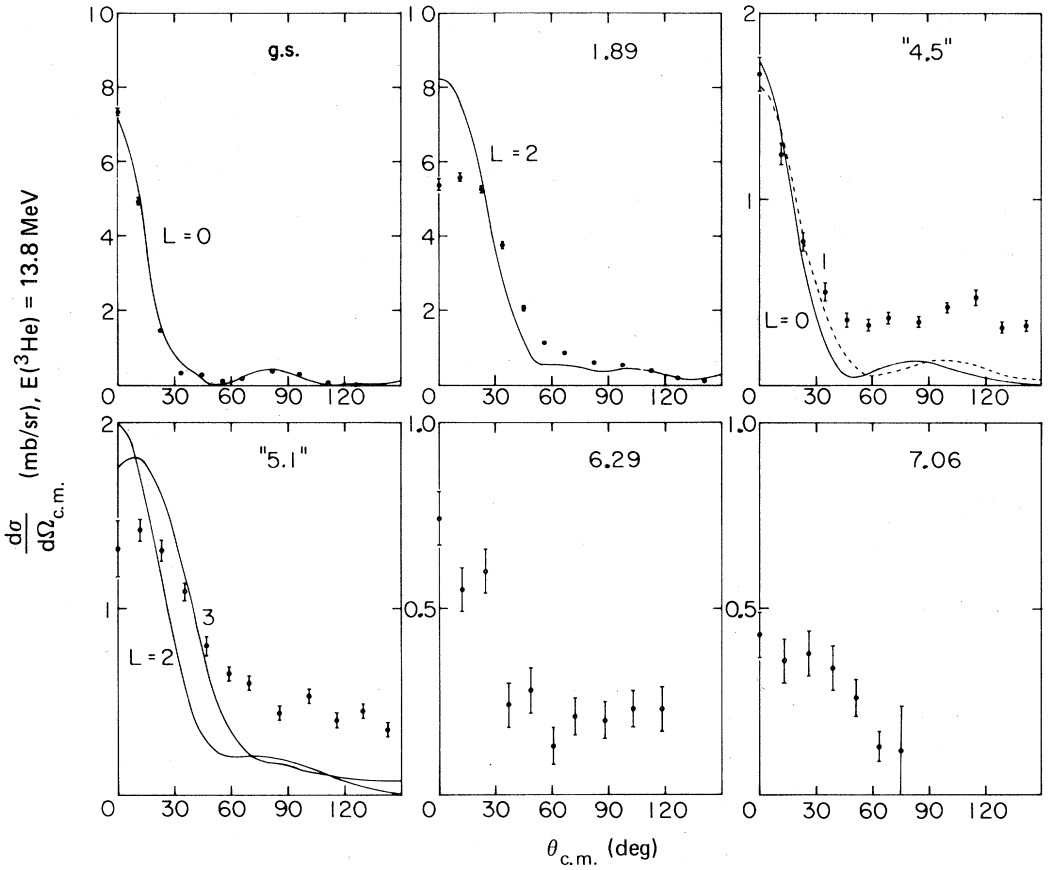


FIG. 9. Angular distributions from $^{16}O(^3He,n)^{18}Ne$ at 13.8 MeV. Smooth curves are the results of DWBA calculations using set II (Table II). The curves are labeled by the angular momentum transfer $L$. Overall uncertainty in the cross section scale is $\pm 15\%$.

large scattering chamber associated with the Princeton AVF cyclotron. The cylindrical gas cell, described in previous work,[43] has a diameter of 3.08 cm and was wrapped by a single 8 $\mu$m Kapton foil, through which the proton beam and the outgoing particles passed. The foil withstood a beam current of 500 nA provided the cell was periodically rotated to expose fresh areas of the foil. The smallest laboratory scattering angle available with this arrangement was 10°. The gas pressure was typically 100 Torr.

The particle telescope consisted of $\Delta E$, $E'$, and veto surface barrier detectors, with typical thicknesses of 200, 2000, and 2000 $\mu$m, respectively. Events were processed by an on-line computer which sorted the particles by type using a range-table look-up procedure. The energy spectra accumlated were written onto magnetic tape for later analyisis on a larger computer system.

Peak positions were obtained by a centroid calculation, or by fitting a standard peak shape to the observed group. Excitation energies were calculated by calibrating the spectrum using the peak positions of known states in $^{14}O$ and $^{10}C$ in $(p,t)$ spectra accumulated when the $^{20}Ne$ was replaced by $CO_2$.

Yields were obtained by fitting with a standard line shape. For groups corresponding to doublets that were not well resolved, the fitted peaks were constrained to have a constant excitation energy difference independent of angle. (In the case of the 3.6 MeV doublet, unconstrained fits gave separations that were slightly more or less, depending on the particular run, than the value expected from the previously measured 40 keV separation.) Cross sections were calculated using the effective solid angle appropriate to our slit geometry.[44]

### B. Experimental results

A $^{20}Ne(p,t)^{18}Ne$ spectrum accumulated at a beam energy of 41.8 MeV and $\theta_{lab} = 20°$ is shown

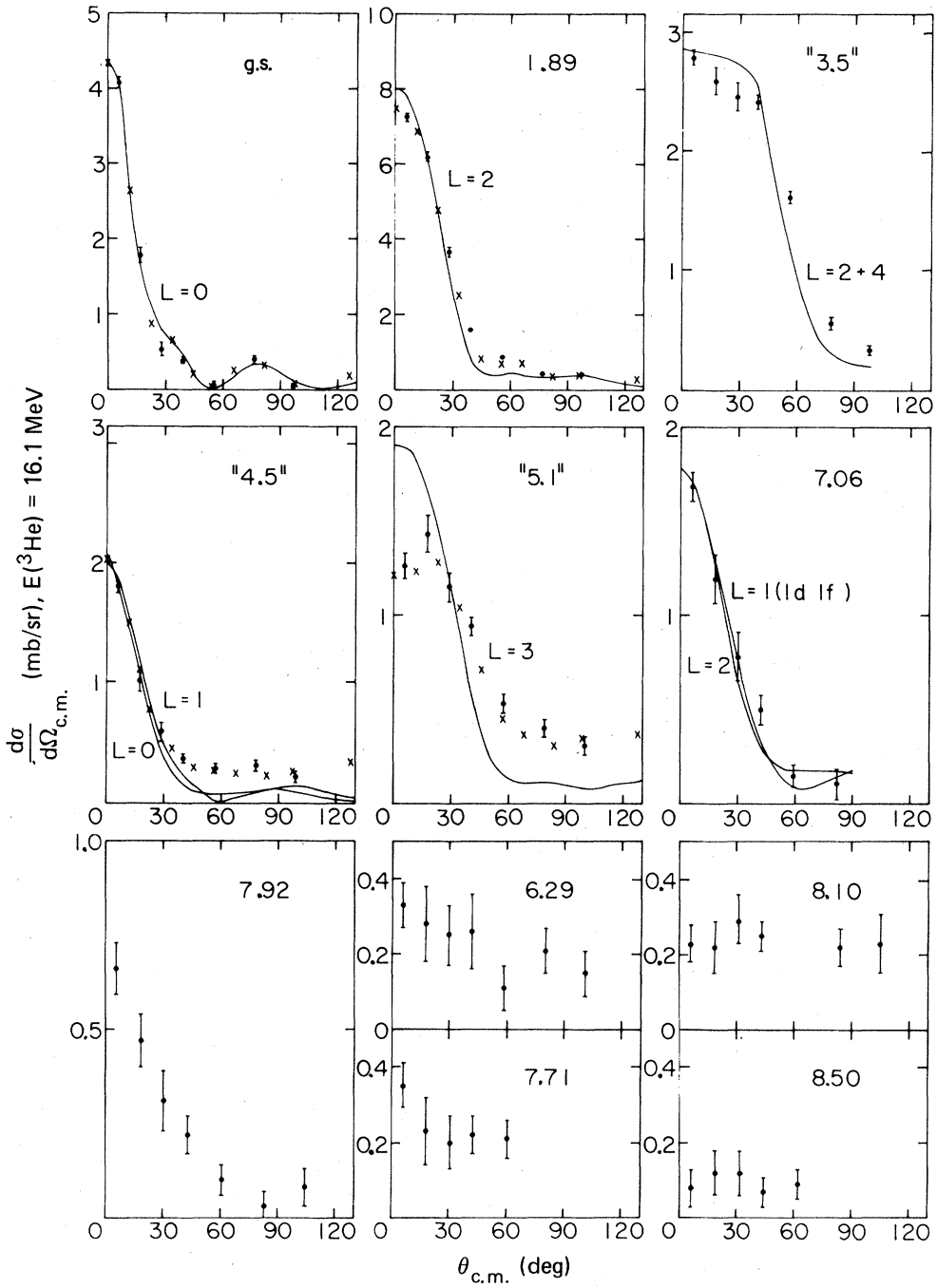


FIG. 10. Angular distributions from $^{16}$O($^3$He,$n$)$^{18}$Ne at 16.1 MeV. Results from 16.3 MeV are superimposed × 's. Smooth curves are DWBA calculations using potential set II (Table II).

in Fig. 12. The states labeled with excitation energies are observed at essentially every angle studied in the range $\theta_{lab} = 10°$ to 40°. On the basis of both the strength of the states and their kinematic behavior, these are evidently states in $^{18}$Ne. Those most strongly populated are the well-known groups below 4 MeV excitation energy, the clear doublet at 4.5 MeV, a group at 5.1 MeV that can be seen to be a doublet because of the shoulder that consistently appears on the high-channel side, a doublet at 6.3 MeV, and a state at 9.2 MeV (not shown). In addition, weaker states were observed at 5.4, 7.7, and

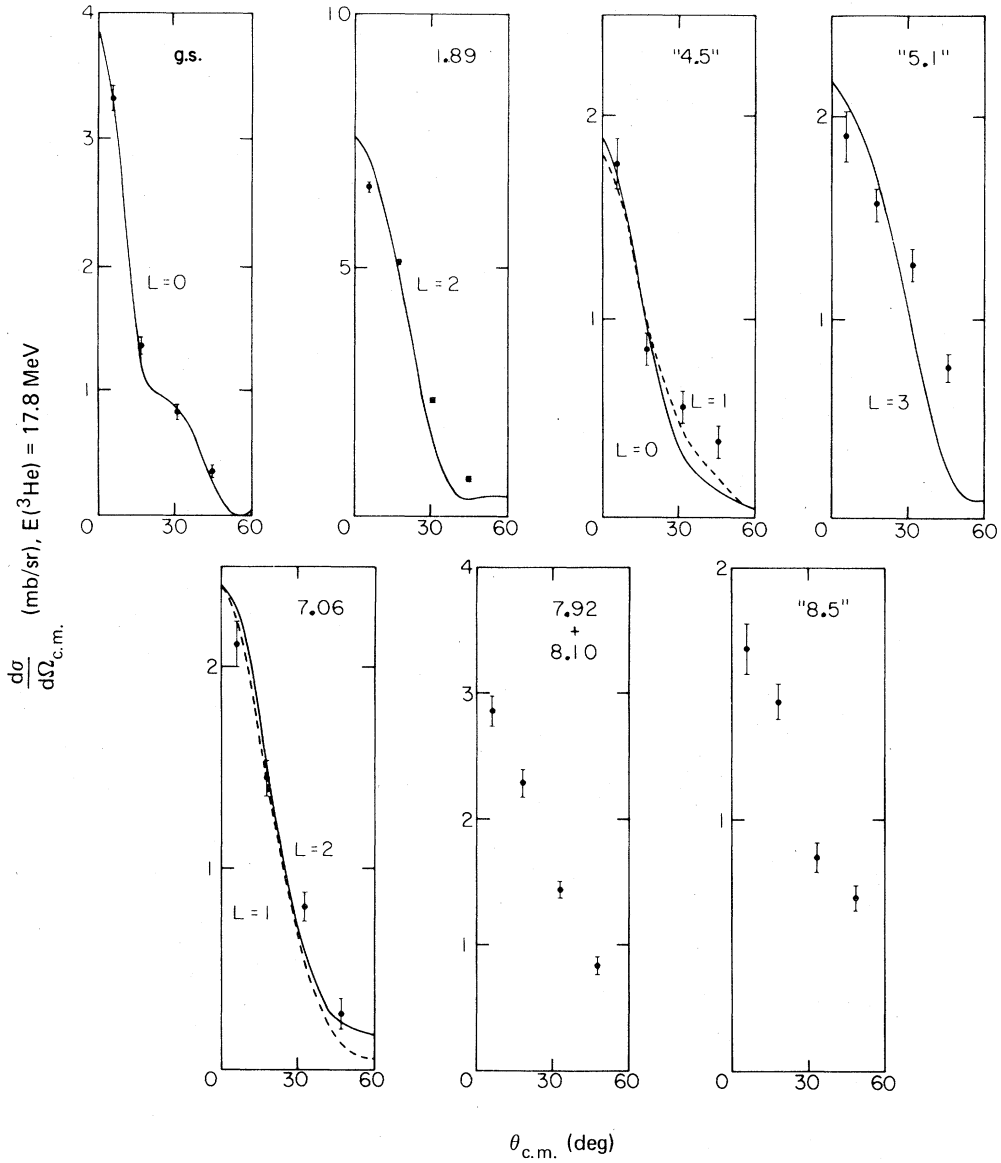


FIG. 11. Angular distributions from $^{16}O(^3He,n)^{18}Ne$ at 17.8 MeV. Smooth curves are DWBA calculations using potential set II (Table II).

7.9 MeV. Measured excitation energies are given in Table I.

Better separation of the 3.6, 4.5, and 5.1 MeV doublets was obtained as a by-product of a remeasurement of the mass of $^{18}Ne$.[45] Using a gas target with the Princeton quadrupole-dipole-dipole-dipole (QDDD) magnetic spectrometer, each doublet was clearly resolved in a single spectrum, shown in Fig. 13. (The segments in the figure were independently accumlated at different field settings.) This measurement confirmed the 5.1 MeV doublet separation of 60 keV, and gave widths for the 5.09 and 5.14 MeV states of $25 \pm 15$ and $40 \pm 20$ keV, respectively.

For states through 4.5 MeV, angular distributions extracted from the telescope data are displyed in Fig. 14. Angular distributions of both members of the 3.6 MeV doublet can be obtained unambiguously because their separation is well known and the width of each member is much less than the experimental resolution.

## IV. DWBA ANALYSIS

The $(^3He,n)$ and $(p,t)$ reaction may be regarded as the transfer of a spin zero, isospin one particle

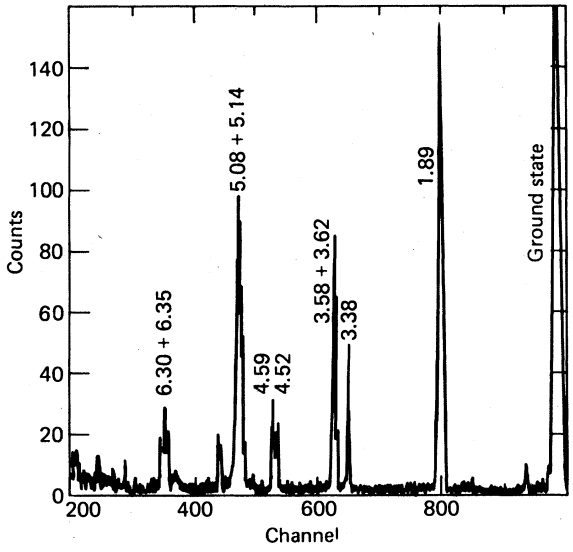


FIG. 12. Counter-telescope spectrum from $^{20}$Ne$(p,t)^{18}$Ne reaction at 41.8 MeV, $\theta_{lab} = 20°$.

pair. For the case of a spin zero target, such as $^{16}$O or $^{20}$Ne, the cross section for a direct, one-step transfer can be shown[46] to equal the square of a sum of transfer amplitudes, each characterized by the same orbital angular momentum transfer $L$. For a direct one-step transition in which compound nuclear processes can be neglected, the angular distribution will have shape characteristic of $L$, and the state being populated must have spin and parity, $J^\pi = 1^{(-1)^L}$. Identification of $L$ therefore determines the spin and parity of the final state, whether made on the basis of a DWBA calculation or by comparison with known transitions.

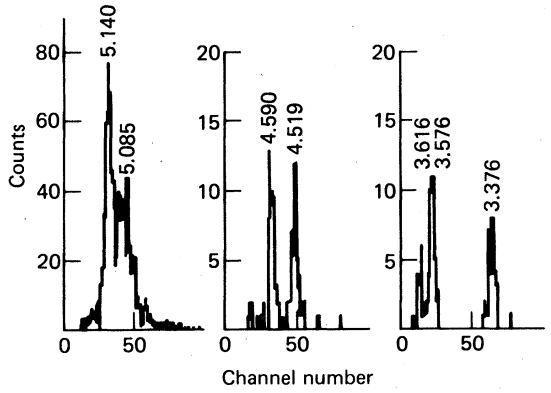


FIG. 13. Results of QDDD spectrograph runs on $^{20}$Ne$(p,t)^{18}$Ne at 41.8 MeV, $\theta_{lab} = 20°$. Peaks are labeled by excitation energies.

### A. Analyis of the $^{16}$O($^3$He,$n$)$^{18}$Ne reaction

DWBA angular distributions were computed using the code JULIE. The computation requires calculation of radial wave functions for the transferred particle pair. For the ($^3$He,$n$) reaction, we calculated this radial function for an unstructured diproton, bound by the diproton separation energy for the state being populated. This is clearly unrealistic if the two protons are stripped into different orbitals. Moreover, if the final state is unbound to particle decay, the calculated stripping amplitude does not converge, so that absolute cross sections are difficult to calculate reliably; the appropriate techniques have not been developed for two-particle transfer reactions. Because we only seek to identify the angular momentum transfer $L$, and because the shape of the angular distribution is not very sensitive to the binding energy for unbound states, we have used a radial wave function corresponding to a barely bound diproton in these cases.

Except where specified below, even $L$ transitions were assumed to involve two $2s$ $1d$ orbitals, and odd $L$ one $2s$ $1d$ and one $1p$ orbital. Elastic scattering of incoming and outgoing particles was calculated using optical potentials (Table II) that are "normal" in the sense that $V \simeq 50$ MeV/nucleon. Set I is that used by Glover and Jones[47,48] to analyze the $^{16}$O$(p,t)$ data of Middleton and Pullen.[14] Set II consists of an incoming potential used in analysis of the $^{18}$O($^3$He,$\alpha$)$^{17}$O reaction[49] and an extrapolation of Perey's potential[50] for the outgoing neutrons.

The curves shown in Figs. 9 to 11 resulted from the use of set II, which gave results that agreed well with data for states with known spin, particularly the ground and first excited states. However, this potential has a tendency to produce a distribution that is too high at small scattering angles, as seen in the $L = 2$ transition to the first excited state and in the mixed transition to the "3.5" MeV group (Fig. 10).

A comparison of the cross section data and the calculated curves leads to the following conclusions: The 4.59 MeV state, which dominates the cross section of the 4.5 MeV doublet at angles less than 30°, is populated by an $L = 0$ or 1 transition. For the 5.1 MeV doublet, $L = 3$ successfully reproduces the drop in cross section at 45° at all bombarding energies studied, but we were not able to determine which member of the doublet should be assigned this value of $L$. The angular distribution to the 7.06 MeV state is reasonably well fit by $L = 1$ or 2 (the $L = 1$ curves being calculated assuming particles in

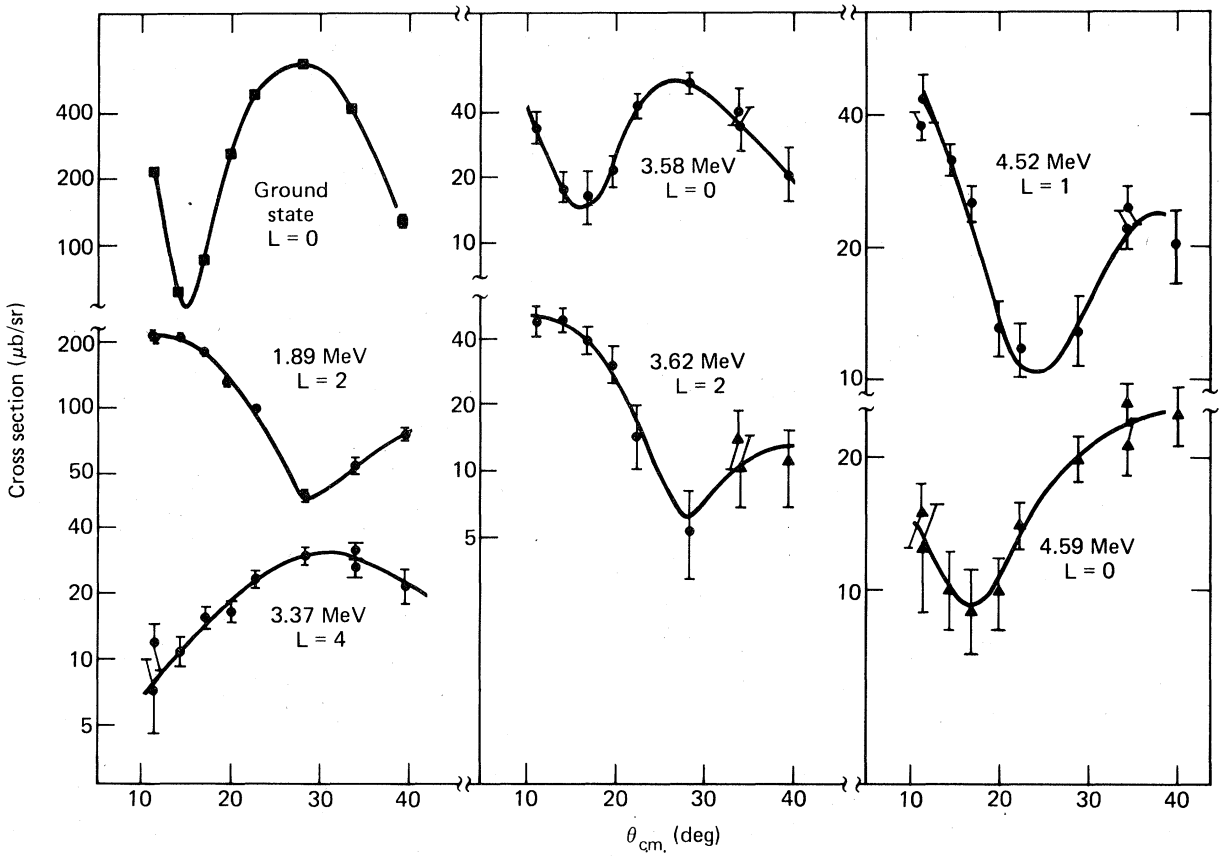


FIG. 14. Angular distributions of $^{20}$Ne$(p,t)^{18}$Ne reaction at 41.8 MeV. Cross section scales have 15% uncertainty. The smooth curves are to guide the eye.

$1d$ and $1f$ orbitals). It also appears probable that the 7.92 MeV state is populated by $L = 0$ or 1 (see Figs. 10 and 11).

### B. Analysis of the $^{20}$Ne$(p,t)^{18}$Ne reaction

As with the ($^3$He,$n$) reaction, we have used the $(p, t)$ angular distributions only for identification of $L$. The DWBA calculations of previous work[17,30] are appropriate, particularly since the calculations of Falk *et al.*[30] were performed for $E_p = 42.6$ MeV, close to the energy of our work, and for all states up to and including the 5.1 MeV doublet.

The spins and partities of the particle-bound states of $^{18}$Ne were known prior to any $(p, t)$ work. Fig-

TABLE II. Optical potentials[a] for distorted wave calculations.

| | Set | $V$ | $r_V$ | $a_V$ | $W_D$ | $W_S$ | $r_W$ | $a_W$ | $r_C$ | Ref. |
|---|---|---|---|---|---|---|---|---|---|---|
| I | in ($^3$He) | 146.8 | 1.40 | 0.55 | 18.4 | | 1.40 | 0.55 | 1.25 | 47 |
| | out ($n$) | 54.4 | 1.20 | 0.51 | 20.0 | | 1.20 | 0.30 | 1.25 | 48 |
| II | in ($^3$He) | 165.1 | 1.22 | 0.80 | 9.96 | | 2.17 | 0.80 | 1.30 | 49 |
| | out ($n$) | $V(E_{\text{c.m.}})$[b] | 1.25 | 0.65 | | 36.6 | 1.25 | 0.47 | 1.25 | 50 |

[a]Potentials have the form

$$V(r) = V_C(r) - V[1/(1+e^x)] - i(W_D - W_S\frac{d}{dx'})[1/(1+e^{x'})],$$

where $x = (r - r_V M_A^{1/3})/a_V$, $x' = (r - r_W M_A^{1/3})/a_W$, and $V_C(r)$ is the Coulomb potential of a uniformly charged sphere of radius $r_C M_A^{1/3}$. Potentials are in MeV; $r$ and $a$ are in fm.

[b]$V(E_{\text{c.m.}}) = 57.2$ MeV $- 0.55E_{\text{c.m.}}$.

ure 14 presents the first experimental data showing that the 3.58 MeV state is populated with an $L = 0$ transfer, as is the ground state, and that the 3.62 MeV state is populated via $L = 2$, as is the 1.89 MeV state. The relative intensities are $\sigma(0_2^+)/\sigma(0_1^+) \simeq 12$ and $\sigma(2_2^+)/\sigma(2_1^+) \simeq 4$.

The angular distributions to the 4.52 and 4.59 MeV states may be compared with the distributions to the lower states and with previous calculations.[30] The observed $L = 0$ transitions to the ground state and 3.58 MeV state, and calculated $L = 0$ shapes, have a minimum around 15°, center of mass. Calculated $L = 1$ transitions have the first minimum at $\simeq 25°$. We conclude that the 4.52 MeV state is populated by an $L = 1$ transfer, and the 4.59 MeV state by $L = 0$. Falk *et al.* concluded, on the other hand, that the doublet (unresolved in their work) was fit by a pure $L = 1$, i.e., that their experimental angular distribution contained no "significant" $L = 0$ strength. However, even their data would be better fitted by a combination of $L = 0$ and 1 (in about the ratio found in the present work) than by a pure $L = 1$, particularly in the vicinity of the minimum that occurs around 22°. Preliminary analysis of observed angular distributions shows only that the two members of the 5.1 MeV doublet are populated with comparable strength.

## V. DISCUSSION

### A. Low-lying particle-unbound levels in $^{18}$Ne

In the $^{16}$O$(t,p)^{18}$O reaction[14] to states between 4 and 6 MeV excitation energy, the weakest transition populates the 4.45 MeV $1^-$ state and the strongest is the $L = 0$ transition to the 5.33 MeV $0^+$ state. The 4.5 MeV doublet seen in our ($^3$He,$n$) data includes a state at 4.59 MeV that is strongly populated by $L = 0$ or 1 and a more weakly populated state at slightly lower excitation energy. A comparison with the $(t,p)$ strengths suggests an $L = 0$ assignment for the 4.59 MeV state. This choice is unambiguously comfirmed by the present $(p,t)$ work. Previous studies of the $^{20}$Ne$(p,t)^{18}$Ne reaction[17,30,31] assigned $L = 1$ to the angular distribution of a group at 4.5 MeV excitation energy. However, their data are consistent with a mixture of $L = 0$ and $L = 1$ in the ratio given by the separate angular distributions obtained in the present work, which leads to the assignment of $J^\pi = 1^-$ and $0^+$ for the 4.51 and 4.59 MeV states, respectively.

The doublet at 5.1 MeV was not resolved in previous work, but Falk *et al.*[30] state that a combination of $L = 2$ and 3 best fits the angular distribution they obtain in the $^{20}$Ne$(p,t)^{18}$Ne reaction. This is consistent with the present observation of a doublet at this energy and the assignment of $L = 3$ as the dominant angular momentum transfer in the ($^3$He, $n$) reaction.

It is instructive to make a comparison with the analogous levels seen in the $^{16}$O$(t,p)^{18}$O reaction,[14] in which states at 5.09, 5.25, and 5.34 MeV are populated with $L = 3$, 2, and 0 respectively. The resulting assignments of $3^-$, $2^+$, and $0^+$ have been confirmed in subsequent work.[5] The weakly populated state at 4.45 MeV was found in this later work to have $J^\pi = 1^-$. The $3^+$ state at 5.37 MeV (Ref. 51) was seen weakly in the $(t,p)$ work. We have already identified the analogous $1^-$ and $0^+$ levels as the 4.5 MeV doublet in $^{18}$Ne. The work of Falk *et al.* and the present work indicate $L = 2$ and 3 strength to the 5.1 MeV doublet, presumably the analogs of the above-mentioned $2^+$ and $3^-$ states of $^{18}$O. The spin parity of particle-bound state (those below 4 MeV in $^{18}$Ne) are known from previous work. These states, together with the doublets at 4.5 and 5.1 MeV, contain the analogs of all the states in $^{18}$O below 5.5 MeV, with the exception of the 5.37 MeV $3^+$ state, which we do not expect to observe in this work because of the $J^\pi = L^{(-)^L}$ selection rule. These states are those of greatest interest for comparison with shell models for mass 18.

### B. Coulomb shifts in mass 18

The 4.59 MeV state of $^{18}$Ne lies 0.75 MeV lower than its analog, the 5.34 MeV state of $^{18}$O. As discussed below ( and in Ref. 34), the observed excitation energy shifts in mass 18 can be used to choose among the various wave function sets that are available by comparing these shifts with the effects expected from the Coulomb force alone, neglecting any other possible charge symmetry violating forces.

In considering the 0.72 MeV shift of the first $\frac{1}{2}^+$ state of mass 13, relative to the ground state, Thomas[52] and Ehrman[53] pointed out that a large relative difference can occur in "single-particle" states when the $R$-matrix energy shift $\gamma^2 L$ is large. The reduced width $\gamma^2$ is related to the size of the single-particle wave function near the nuclear surface; $L$ is the logarithmic derivative of the exterior wave function at the surface. Single-particle wave functions can have quite different boundary values for neutrons and protons, leading to the possibility

of large shifts in mirror nuclei. This is particularly true if the $s_{1/2}$ orbital is involved, since the additional Coulomb energy associated with a proton easily alters the radial wave function, which extends particularly far from the nuclear center. This phenomenon has also been treated more simply[54,55] by calculating the energy of this last particle in a Woods-Saxon nuclear potential (plus a Coulomb potential when the particle is a proton); in this way energies, and hence Coulomb shifts, are obtained naturally. We use this approach, extending it to a "two-particle" system, mass 18. Coulomb energies in mass 18 have been discussed in previous work,[18–20] but only Kahana[20] made a comprehensive attempt to treat the low-lying $T = 1$ states of mass 18. Presuming that most of the $s_{1/2}{}^2$ strength lay in the $0_2^+$ state, he calculated a Coulomb shift for that state that was much larger than that observed experimentally. He did not treat $0_3^+$. On the other hand, Adelberger and McDonald[25] and Rolfs *et al.*,[56] in discussing the third $J^\pi = 0^+$, $T = 1$ multiplet, pointed out that the large shift in these states could be accounted for by a double Thomas-Ehrman shift associated with a predominantly $s_{1/2}{}^2$ configuration. We shall apply our technique to the states that are expected to contain configurations constructed primarily of the $2s_{1/2}$ and $1d_{5/2}$ orbitals and of the lowest $0^+$, $2^+$, and $4^+$ deformed structures.

We calculate relative Coulomb shifts in terms of the radial wave function differences in the two-particle components of the state vector. We write the state $\alpha$, with spin $J$, as

$$|\alpha J\rangle = \sum_{j_2 \geq j_1} c_{j_1 j_2}^{\alpha J} |j_1 j_2 J\rangle + \sum_i A_i^{\alpha J} |p^{-2} i J\rangle ,$$

where the first term consists of configurations with two particles (with spins $j_1$ and $j_2$ in the *sd* shell) and the second term of "hole" configurations with spin $J$. The latter are "deformed" structures resembling $^{20}$Ne states less two $p$-shell particles. We assume that the Hamiltonian in the two-particle subspace is $H_{nn} = T_1 + T_2 + V_1 + V_2 + V_{12}$ for $^{18}$O and $H_{pp} = H_{nn} + W_1 + W_2 + W_{12}$ for $^{18}$Ne, where the $V$'s and $W$'s are nuclear and Coulomb potentials, respectively. We assume that the configuration amplitudes remain the same across $T = 1$ multiplets, but that the radial wave functions may change, particularly in the surface and external regions. Forming the difference $\langle \alpha J^{nn} | H_{pp} | \alpha J^{pp} \rangle - \langle J^{pp} | H_{nn} | \alpha J^{nn} \rangle$ *for a pure two-particle case* (i.e., assuming $A_i^{\alpha J} = 0$) and integrating out to a radius $R$ near the nuclear surface, we obtain

$$E_{pp} - E_{nn} = \frac{\sum_{j_2 \geq j_1} (c_{j_1 j_2}^{\alpha J})^2 [\theta(j_1)\Delta_{j_i} + \theta(j_2)\Delta_{j_2}]}{\sum_{j_2 \leq j_1} (c_{j_1 j_2}^{\alpha J})^2 \theta(j_1)\theta(j_2)} + \frac{\langle \alpha J^{pp} | W_{12} | \alpha J^{nn} \rangle_R}{\langle \alpha J^{pp} | \alpha J^{nn} \rangle_R} ,$$

where

$$\Delta_{j_1} = \langle u_p^{j_1} | W_{j_1} | u_n^{j_1} \rangle_R - \frac{\hbar^2}{2mR} [u_p^{j_1}(R) u_n^{j_1}(R)](L_p^{j_1} - L_n^{j_1})_R ,$$

$$\theta(j_1) = \langle u_p^{j_1} | u_n^{j_1} \rangle_R ,$$

and $E_{pp}(E_{nn})$ is the eigenvalue of $H_{pp}(H_{nn})$ for the state $\alpha J$. Corrections to $E_{pp} - E_{nn}$ of order $(m_p - m_n)/(m_p + m_n)$ have been neglected. The subscript $R$ indicates the limit of the radial integration. We have written single-particle wave functions as $[u(r)/r]x(\chi,\Omega)$, where $\chi$ and $\Omega$ are spin and angular coordinates. $L$ is the logarithmic derivative $u^{-1}du/dr$.

The $\Delta_{j_1}$ have the form of the Coulomb energy differences one would obtain by performing the above exercise for a one-particle case: The first term is the first order energy; the second is the Thomas-Ehrman energy shift $\gamma^2(L_p - L_n)$. In the two-particle case, replacing simple neutron-proton overlap integrals by 1, we write

$$E_{pp} - E_{nn} = \sum_{j_2 \geq j_1} (c_{j_1 j_2}^{\alpha J})^2 (\Delta_{j_1} + \Delta_{j_2}) + 2\delta \sum_i (d_i^{\alpha J})^2 + \langle \alpha J | W_{12} | \alpha J \rangle ,$$

where $\Delta_j$ is $(E_p - E_n)_j$, the one-particle Coulomb difference for the $j$ orbital, and we have now added a term arising from hole configurations, all of which are assigned an equivalent single particle shift $\delta$. The last term is the two-particle Coulomb energy $\langle W_{12} \rangle$ for the wave function under consideration.

We evaluate $\Delta_j$ from a potential model including the "dominant" terms of Ref. 55. In order to simulate the boundary effects properly, we choose parameters appropriate to the separation of a nucleon from a mass 17 core. As an example, $E_p - E_n$ for the $s_{1/2}{}^2$ component in a $0^+$ wave function is evaluated by adjusting the nuclear well depth to produce the *observed* binding with respect to $n + {}^{17}\mathrm{O}$ ($\frac{1}{2}^+$, $E_x = 870$ keV), of an $s_{1/2}$ neutron in the $^{18}$O state in question. The Coulomb potential is then added to this nuclear part, and the

binding of a proton is *calculated,* yielding $\Delta_{s_{1/2}} = E_p - E_n$. In this case, we are effectively calculating the binding of a proton in $^{18}$Ne with respect to $p + {}^{17}\mathrm{F}(\frac{1}{2}^+, E_x = 500$ keV). The potential well size parameters and the spin-orbit strength are taken from Ref. 57. The Coulomb potential is derived from the charge distribution parameters of Ref. 58. The single-particle shifts include corrections for the electromagnetic spin-orbit energy difference and the Coulomb exchange energy as in Ref. 55. For $2s_{1/2}$ and $1d_{5/2}$ orbitals, Fig. 15 shows $E_p - E_n$ vs $E_n$, the neutron energy with respect to $^{17}\mathrm{O} + n$. The single-particle Coulomb exchange energy is shown separately in the lower portion of Fig. 15. Performing the proton calculation with a $Z = 9$ mass 17 core has included—in an average way—some Coulomb energy which will be included explicitly in $\langle W_{12} \rangle$. Accordingly, we subtract from the single-particle shifts $\frac{1}{9}$ of the separately calculated Coulomb energy for the case under consideration. Given the experimental $^{18}$O spectrum and a set of wave functions, the first term of $E_{pp} - E_{nn}$ may then be evaluated for each state by using the expression stated above.

The valence Coulomb interaction energy $\langle W_{12} \rangle$ was explicitly calculated only for the amplitudes of Benson and Flowers,[10] using the radial wave functions from the potential discussed above. The small $d_{3/2}$ configurations were retained only in this portion of the calculation. We have neglected the deformed configurations, which are less than 10% of the wave functions in all but $0_2^+$ and $2_3^+$ states. The values of $\langle W_{12} \rangle$ for the five states that are predominantly two-particle configurations are shown in Fig. 16. It is useful to note that the range in values is due, in roughly comparable degrees, to both the *configuration* dependence of $\langle W_{12} \rangle$ and to its *binding energy* (or, equivalently, size) dependence. To take account of the presence of deformed configurations, these values were augmented by $\sum_i d_i^2$ times 380 keV, roughly the average Coulomb interaction energy calculated for the two-particle configurations.

Using our expression for $E_{pp} - E_{nn}$, we can then calculate the Coulomb shift for the Benson and Flowers wave functions as a function of $\delta$. In the calculation of the $\sum (c_{j_i j_2}^{\alpha J})^2 (\Delta_{j_1} + \Delta_{j_2})$ term, only configurations including the $2s_{1/2}$ and/or $1d_{5/2}$

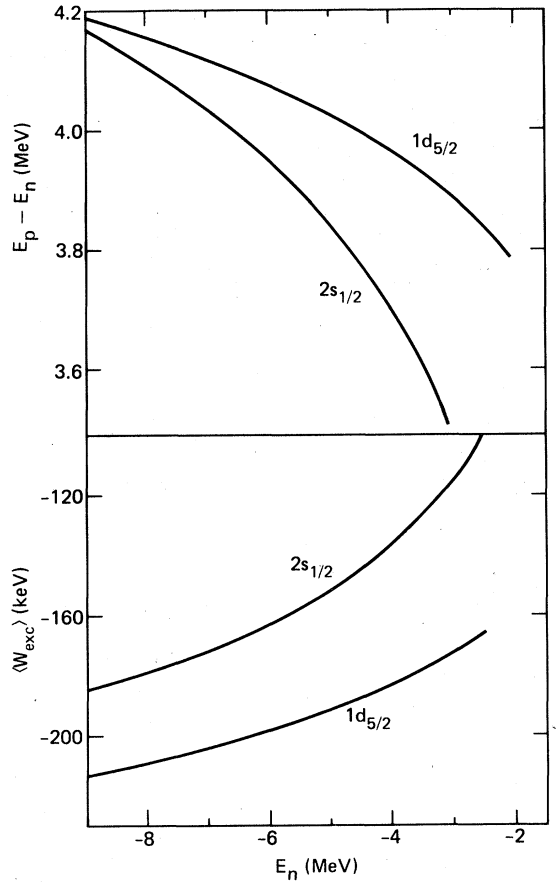


FIG. 15. Single-particle shifts $E_p - E_n$ (including electromagnetic spin-orbit energy) and Coulomb exchange energy ($W_{exc}$), for $2s_{1/2}$ and $1d_{5/2}$ orbitals, as a function of neutron single-particle energy $E_n$.

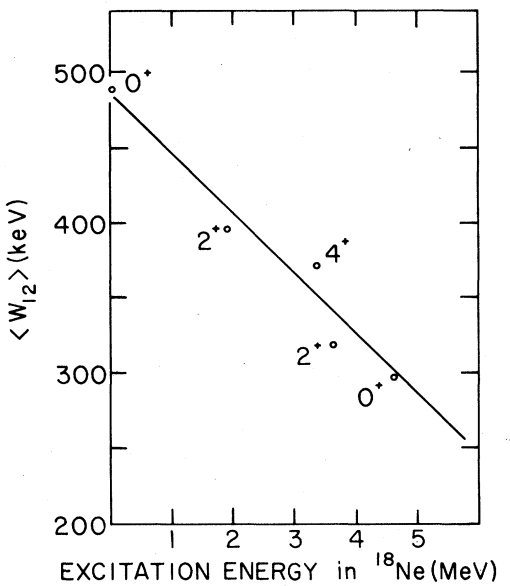


FIG. 16. Coulomb correlation energy (using wave functions of Ref. 10 ) for predominantly two-particle states, as a function of energy in $^{18}$Ne.

single-particle orbitals are included. *All other* amplitudes are lumped into the $\sum_i d_i{}^2$ term. (The next highest single-particle orbital is $d_{3/2}$, which dominates a state near 5 MeV in mass 17; the low-lying levels of mass 18 are so deeply bound relative to this state that wave function components involving $d_{3/2}$ would not be expected to exhibit sizable "Thomas-Ehrman" shifts. In this respect, these components might act similarly to deformed components, which are also, in effect, deeply bound, so that lumping them together is appropriate.) Selection of a value for $\delta$ produces, for a given state in $^{18}$O, a value for $E_{pp}-E_{nn}$; when added to the binding of the state in $^{18}$O, this yields the binding in $^{18}$Ne. The absolute value calculated for this binding is not expected to be precise but the *relative* values for the binding (or excitation energies) of states in $^{18}$Ne should be accurate to 100 keV or less.

The method of choosing $\delta$ to give the $^{18}$Ne level diagram is demonstrated in Fig. 17 for the wave functions of Ref. 10. For each state, we plot the energy relative to $^{16}$O + 2$p$ vs $\delta$. The two low-lying levels that are predominantly deformed structures according to Ref. 10 change most rapidly in energy as $\delta$ is varied. A value of $\delta = 3450$ keV,

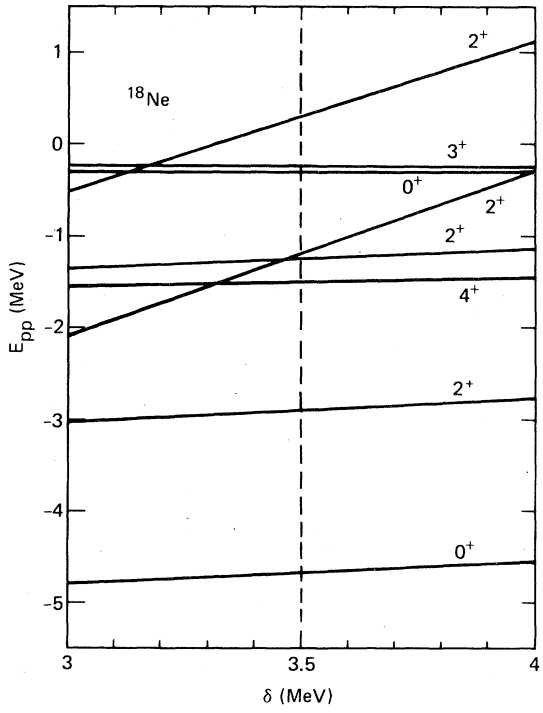


FIG. 17. Total calculated binding energy for $^{18}$Ne as a function of the "deformed single-particle shift" parameter $\delta$, using wave functions of Ref. 10.

TABLE III. Excitation energies of $T = 1$ states in $^{18}$O and $^{18}$Ne.[a]

| $J^\pi$ | $^{18}O_{expt}$[b] | $^{18}Ne_{expt}$ | $^{18}Ne_{calc}$[e] | $\Delta$[f] |
|---|---|---|---|---|
| $0_1^+$ | 0 | 0 | 140 | +140 |
| $2_1^+$ | 1982 | 1887[c] | 1911 | + 24 |
| $4_1^+$ | 3555 | 3376[c] | 3325 | − 50 |
| $0_2^+$ | 3634 | 3576[c] | 3546 | − 28 |
| $2_2^+$ | 3921 | 3616[c] | 3575 | − 41 |
| $2_3^+$ | 5260 | 5113[d] | 5055 | − 58 |
| $0_3^+$ | 5336 | 4590[d] | 4550 | − 40 |

[a]All energies in keV.
[b]From Reference 59.
[c]From Reference 5.
[d]From present work. 5113 is the mean of states in the 5.1-MeV doublet.
[e]3450 keV; see text.
[f]$\Delta = {}^{18}Ne_{calc} - {}^{18}Ne_{expt}$.

selected by matching the experimentally observed positions of $^{18}$Ne states, yields excitation energies given in Table III. In spite of $^{18}$O − $^{18}$Ne shifts as large as 750 keV (for $0_3^+$), the calculated $^{18}$Ne energies compare quite well with the experimental values, the maximum and average absolute discrepancies being 140 and 55 keV, respectively. The $0_2^+$ state, which gave Kahana[20] so much difficulty, is well reproduced here.

Other sets of wave functions were tested as well. These included those of Kuo and Brown,[3] Federman,[9] Federman and Talmi,[13] and Engeland.[7] In each case, at least one state was in error by 350 keV, and the *average* discrepancy was greater than 100 keV (it was 170 keV for those of Ref. 7). Wave functions such as those of Benson and Flowers, which place most of the $s_{1/2}{}^2$ strength in the state $0_3^+$ observed at 4.5 MeV in $^{18}$Ne, are strongly preferred. Those of Ellis and Engeland[11] should give similar results. A similar test can be applied to a comparison of observed $T = 1$ states in $^{18}$F with calculations referred from $^{18}$O. This has the advantage that $\langle W_{12} \rangle$ does not appear in the expression for $E_{np} - E_{nn}$, but the relative Coulomb shifts are generally smaller. The conclusions are similar to those stated above.

### C. Higher levels in $^{18}$Ne

In addition to studying the states up to 5.1 MeV in $^{18}$Ne, the present work has identified states at 5.45, 6.30, 6.35, 7.06, 7.71, 7.92, 7.95, 8.10, 8.50, and 9.20 MeV; the 6.30, 7.95, and 9.20 MeV states had been seen in previous $^{20}$Ne($p$, $t$) studies. From the ($^3$He, $n$) angular distributions, the 7.06 and 7.92

MeV states appear to be populated with angular momentum transfers of 1 or 2 suggesting $1^-$ or $2^+$ assignments. Of the $(p, t)$ results for the high-lying states, Falk *et al.*[30] ascribe a $L = 4$ transfer to the 6.30 MeV state, suggesting $J^\pi = 4^+$. The data are not persuasive in suggesting assignments for other states.

As seen in Table I, the pickup and stripping reactions leading to $^{18}$Ne populate largely disjoint sets of states at these higher excitation energies. The 7.06 MeV state, distinctly populated via $(^3\text{He}, n)$, is not seen at all in the $(p, t)$ reaction. Such selective population would be expected on the simplest grounds, assuming one-step direct reactions. In a model where the $^{16}$O ground state is a closed core and the $^{20}$Ne ground state is a pure $d_{5/2}{}^4$ configuration, the $(^3\text{He}, n)$ reaction can only populate two-particle states constructed by putting protons in $d_{5/2}$, $s_{1/2}$, $d_{3/2}$,. . . orbitals. On the other hand, the only two-particle configuration that $(p, t)$ can easily populate is $d_{5/2}{}^2$; but $(p, t)$ can also directly populate more complicated configurations involving, for example, holes in the $p$ shell. The state at 7.06 MeV is a good candidate for substantial $d_{3/2}$ strength, since it may have an admissible spin and parity $(2^+)$ and it is strongly populated by $(^3\text{He}, n)$ but not by $(p, t)$. However, there is no evidence for such states in $^{18}$O. Above 5.5 MeV excitation, the only $^{18}$O state whose structure has been suggested by any experimental evidence is the $4^+$ state at 7.10 MeV, which is apparently dominated by "deformed" configurations. No apparent analog for this state has been identified in $^{18}$Ne.

### D. Structure of mass 18

Several types of experimental evidence may now be brought to bear on the question of the structure of $T = 1$ states in mass 18: one- and two-particle transfer strengths, gamma transition rates (and multipolarity), and Coulomb energy shifts. As discussed above, the very existence of three $0^+$ and three $2^+$ states at low excitation energy and observation of enhanced $E2$ transition rates suggested the presence of deformed configurations in this region, in addition to two-particle configurations based on $d_{5/2}$ and $s_{1/2}$ orbitals.

Observed particle transfer strengths were consistent with this picture, but did not unambiguously identify which of the $0^+$ states carries most of the deformed strength. However, the Coulomb shifts observed in the present work require that $0_3^+$ carry the $s_{1/2}{}^2$ strength and therefore that most of the deformed strength be assigned to $0_2^+$. Subsequent examination of particle-stripping strengths to $^{18}$O $0^+$ states indicate that only this view is consistent with all the data.[35,36] It is also favored by a recent analysis of newly measured one-particle stripping strengths to $^{18}$O states.[60] As noted in Ref. 37, the single datum that cannot be reproduced by calculations presuming $0_3^+$ to be predominantly $s_{1/2}{}^2$ is the measured quadrupole moment of $2_2^+$ in $^{18}$O.[61]

This establishes the major features of low-lying $T = 1$ levels in mass 18, but not the importance of the $d_{3/2}$ orbital in this region or the detailed character of the deformed configurations. Calculations are also able to write the deformed configurations in terms of complicated particle-hole structure.[62,63] However, no single calculation has dealt successfully with both $d_{3/2}$ and deformed configurations.

We should reemphasize, though, that the main features of states in the 0 to 5 MeV range are now clear, because this fact may be obscured by some recent analyses of direct reactions leading to $T = 1$ states in mass 18. Escudié *et al.*[64] conclude—on the basis of inelastic proton scattering on $^{18}$O—that the $0^+$ ground, $2^+$ 1.98 MeV, and $4^+$ 7.10 MeV states constitute a rotational band. Although their data are consistent with such a conclusion, they do not even test the more plausible possibility that the 3.63 MeV $0^+$, 5.25 MeV $2^+$, and 7.10 MeV $4^+$ states resemble a rotational band structurally. The only "band" which the ground state and 1.98 MeV state appear to belong to is the "$d_{5/2}{}^2$" band, which also includes the $4^+$ state at 3.55 MeV. Inevitably, the first $0^+$ and $2^+$ states contain admixtures of members of the band mentioned above, which may explain the results of Ref. 64.

A recent analysis of the $^{20}\text{Ne}(p, t)^{18}\text{Ne}$ reaction attempted to test the Benson and Flowers wave functions using coupled-channel Born-approximation (CCBA) calculations.[65] Unfortunately, attention was restricted to the states below 4 MeV, ignoring the available data[34] on the third $0^+$ state, a state that must be included for a full comparison with these wave functions. The authors also note that their comparison with experimental data might be made firmer by independent angular distributions to the $0_2^+$ and $2_2^+$ states. The first independent data on these states are given in Fig. 14, and a CCBA analysis, beyond the scope of the present work, would be very interesting.

## VI. CONCLUSIONS

Study of the $^{16}\text{O}(^3\text{He}, n)^{18}\text{Ne}$ and $^{20}\text{Ne}$ $(p, t)^{18}\text{Ne}$ reactions has identified new states in $^{18}$Ne beginning

at 5.45 MeV and demonstrated unambiguously that the 4.51 and 5.1 MeV groups observed in previous work are doublets. The 4.5 MeV doublet consists of a $1^-$ and $0^+$ state. Higher states exhibit angular distributions suggestive of population via direct reaction, and certain of these states, in particular the 7.06 MeV $1^-$ or $2^+$ state, may contain substantial $d_{3/2}$ strength, heretofore unseen in $^{18}$Ne. The level diagram of $^{18}$Ne is now sufficiently complete to yield, by comparison with $^{18}$O states, a set of experimental Coulomb energy shifts. We have used a two-particle model for calculating Coulomb energies to test proposed sets of wave functions against these observed shifts. Among the wave functions that satisfactorily reproduced particle transfer strengths and gamma transition rates, only those that place most of the $s_{1/2}{}^2$ in the second $0^+$ can reproduce the Coulomb shifts. This serves to fix the main structural features of low-lying $T = 1$ states in mass 18.

This work was supported in part by the National Science Foundation, and in part by the U.S. Department of Energy under Contract No. W-7405-Eng-48.

---

*Present Address: Lawrence Berkeley Laboratory, Berkeley, California 94720.
†Present Address: University of Washington, Seattle, Washington 98195.

[1]J. F. Dawson, I. Talmi, and J. D. Walecka, Ann. Phys. (N.Y.) 18, 339 (1962).
[2]B. H. Flowers and D. Wilmore, Proc. Phys. Soc. London 83, 683 (1964).
[3]T. T. S. Kuo and G. E. Brown, Nucl. Phys. 85, 40 (1966).
[4]A. Arima, S. Cohen, R. D. Lawson, and M. H. Macfarlane, Nucl. Phys. A108, 94 (1968).
[5]F. Ajzenberg-Selove, Nucl. Phys. A190, 1 (1972).
[6]G. E. Brown, C. R. Congr. Int. Phys. Nucl. Paris 1, 129 (1964).
[7]T. Engeland, Nucl. Phys. 72, 68 (1965).
[8]G. E. Brown and A. M. Green, Nucl. Phys. 85, 87 (1966).
[9]P. Federman, Nucl. Phys. A95, 443 (1967).
[10]H. G. Benson and B. H. Flowers, Nucl. Phys. A126, 332 (1969).
[11]P. J. Ellis and T. Engeland, Nucl. Phys. A144, 161 (1970); A181, 368 (1972).
[12]S. Shlomo and R. Moreh, Nucl. Phys. A110, 204 (1968).
[13]P. Federman and I. Talmi, Phys. Lett. 15, 165 (1965); 19, 490 (1965).
[14]R. Middleton and D. J. Pullen, Nucl. Phys. 51, 63 (1964).
[15]F. Donau, K. Hehl, C. Riedel, R. A. Broglia, and P. Federman, Nucl. Phys. A101, 495 (1967).
[16]H. G. Benson and J. M. Irvine, Proc. Phys. Soc. London 89, 249 (1966).
[17]J. L'Ecuyer, R. D. Gill, K. Ramavataram, N. S. Chant, and D. G. Montague, Phys. Rev. C 2, 116 (1970).
[18]G. F. Bertsch, Phys. Rev. 174, 1313 (1968).
[19]C. A. Rappleyea and P. D. Kunz. Nucl. Phys. A139, 24 (1969).
[20]S. Kahana, Phys. Rev. C 5, 63 (1972).
[21]J. H. Towle and B. E. F. Macefield, Proc. Phys. Soc. London 77, 399 (1961).
[22]N. H. Gale, J. B. Garg, and K. Ramavataram, Nucl. Phys. 22, 500 (1962).
[23]M. Krick and G. J. F. Legge, Nucl. Phys. 89, 63 (1966).
[24]J. H. Towle and G. J. Wall, Nucl. Phys. A118, 500 (1968).
[25]E. G. Adelberger and A. B. McDonald, Nucl. Phys. A145, 497 (1970).
[26]B. C. Robertson, R. A. I. Bell, J. L'Ecuyer, R. D. Gill, and H. J. Rose, Nucl. Phys. A126, 431 (1969).
[27]C. Rolfs, W. Trost, F. Reiss, R. Kramer, and E. Kuhlmann, Nucl. Phys. A137, 481 (1969).
[28]M. H. Shapiro, A. Adams, C. Moss, and W. M. Denny, Nucl. Phys. A144, 17 (1970).
[29]J. C. Hardy, H. Brunnader, J. Cerny, and J. Jänecke, Phys. Rev. 183, 854 (1969).
[30]W. R. Falk, R. J. Kidney, P. Kulisic, and G. K. Tandon, Nucl. Phys. A157, 241 (1970).
[31]R. A. Paddock, Phys. Rev. C 5, 485 (1972).
[32]A. V. Nero and E. G. Adelberger, Bull. Am. Phys. Soc. 15, 1686 (1970).
[33]F. S. Dietrich, A. V. Nero, amd G. E. Walker, Bull. Am. Phys. Soc. 15, 1658 (1970).
[34]A. V. Nero, E. G. Adelberger, F. S. Dietrich, and G. E. Walker, Phys. Rev. Lett. 32, 623 (1974).
[35]H. T. Fortune and S. C. Headley, Phys. Lett 51B, 136 (1974).
[36]R. D. Lawson, F. J. D. Serduke, and H. T. Fortune, Phys. Rev. C 14, 1245 (1976).
[37]T. Erikson and G. E. Brown, Nucl. Phys. A277, 1 (1977).
[38]D. Evers, C. Ley, E. Spindler, W. Assmann, K. Rudolph, P. Konrad, and P. Sperr, Nucl. Phys. A275, 363 (1977).
[39]A. V. Nero, Ph. D. thesis, Stanford University, 1970 (unpublished).
[40]J. E. Brolley and J. L. Fowler, in *Fast Neutron Physics*, edited by J. B. Marion and J. L. Fowler (Interscience,

New York, 1960), Part I, Chap. 1C.
[41]W. E. Wilson, R. L. Walter, and D. B. Fossan, Nucl. Phys. 27, 421 (1961).
[42]M. D. Goldberg, J. D. Anderson, J. P. Stoering, and C. Wong, Phys. Rev. 122, 1510 (1961).
[43]R. S. Ohanian, Ph. D. thesis, Princeton University, 1973 (unpublished).
[44]E. A. Silverstein, Nucl. Instrum. Methods 4, 53 (1959).
[45]F. P. Calaprice, S. J. Freedman, and A. V. Nero, private communication.
[46]N. K. Glendenning, Phys. Rev. 137, 102 (1965).
[47]R. N. Glover and A. D. W. Jones, Nucl. Phys. 81, 268 (1966).
[48]R. N. Glover and A. D. W. Jones, Nucl. Phys. 81, 277 (1966).
[49]C. Détraz and H. H. Duhm, Phys. Lett. 29B, 29 (1969).
[50]F. G. Perey, Phys. Rev. 131, 745 (1963).
[51]J. L. Wiza, R. Middleton, and P. V. Hewka, Phys. Rev. 141, 975 (1966).
[52]R. G. Thomas, Phys. Rev. 81, 148 (1951).
[53]J. B. Ehrman, Phys. Rev. 81, 412 (1951).
[54]T. A. Tombrello, Phys. Lett. 23, 134 (1966).
[55]J. A. Nolen, Jr and J. P. Schiffer, Annu. Rev. Nucl. Sci. 19, 471 (1969).
[56]C. Rolfs, W. E. Kieser, R. E. Azuma, and A. E. Litherland, Nucl. Phys. A199, 274 (1973).
[57]B. A. Watson, P. P. Singh, and R. E. Segel, Phys. Rev. 182, 977 (1969).
[58]I. Sick and J. S. McCarthy, Nucl. Phys. A150, 631 (1970).
[59]J. W. Olness, E. K. Warburton, and J. A. Becker, Phys. Rev. C 7, 2239 (1973).
[60]T. K. Li, D. Dehnhard, R. E. Brown, and P. J. Ellis, Phys. Rev. C 13, 55 (1976).
[61]A. M. Kleinfeld, K. P. Lieb, D. Werdecker, and U. Smilansky, Phys. Rev. Lett. 35, 1329 (1975).
[62]A. P. Zuker, Phys. Rev. Lett. 23, 983 (1969).
[63]J. B. McGrory and B. H. Wildenthal, Phys. Rev. C 7, 974 (1973).
[64]J. L. Escudié, R. Lombard, M. Pignanelli, F. Resmini, and A. Tarrats, Phys. Rev. C 10, 1645 (1974).
[65]D. K. Olsen, T. Udagawa, and R. E. Brown, Phys. Rev. C 11, 1557 (1975).